Clim Dyn (2008) 30:485–496
DOI 10.1007/s00382-007-0292-3

Interannual variations of the boreal summer intraseasonal variability predicted by ten atmosphere–ocean coupled models

Hye-Mi Kim · In-Sik Kang · Bin Wang · June-Yi Lee

Received: 9 January 2007 / Accepted: 19 June 2007 / Published online: 18 July 2007
© Springer-Verlag 2007

Abstract The reproducibility of boreal summer intraseasonal variability (ISV) and its interannual variation by dynamical models are assessed through diagnosing 21-year retrospective forecasts from ten state-of-the-art ocean–atmosphere coupled prediction models. To facilitate the assessment, we have defined the strength of ISV activity by the standard deviation of 20–90 days filtered precipitation during the boreal summer of each year. The observed climatological ISV activity exhibits its largest values over the western North Pacific and Indian monsoon regions. The notable interannual variation of ISV activity is found primarily over the western North Pacific in observation while most models have the largest variability over the central tropical Pacific and exhibit a wide range of variability in spatial patterns that are different from observation. Although the models have large systematic biases in spatial pattern of dominant variability, the leading EOF modes of the ISV activity in the models are closely linked to the models' El Nino-Southern Oscillation (ENSO), which is a feature that resembles the observed ISV and ENSO relationship. The ENSO-induced easterly vertical shear anomalies in the western and central tropical Pacific, where the summer mean vertical wind shear is weak, result in ENSO-related changes of ISV activity in both observation and models. It is found that the principal components of the predicted dominant modes of ISV activity fluctuate in a very similar way with observed ones. The model biases in the dominant modes are systematic and related to the external SST forcing. Thus the statistical correction method of this study based on singular value decomposition is capable of removing a large portion of the systematic errors in the predicted spatial patterns. The 21-year-averaged pattern correlation skill increases from 0.25 to 0.65 over the entire Asian monsoon region after applying the bias correction method to the multi-model ensemble mean prediction.

Keywords Intraseasonal variability · ISV activity · ENSO · Predictability · Statistical correction

H.-M. Kim · I.-S. Kang (✉)
School of Earth and Environmental Sciences,
Seoul National University,
Seoul 151-742, South Korea
e-mail: kang@climate.snu.ac.kr

B. Wang · J.-Y. Lee
Department of Meteorology and International Pacific Research Center, University of Hawaii at Manoa,
Honolulu, HI, USA

1 Introduction

Interannual variability of the Asian monsoon has been considered an important issue because of its social and economic impact on populations and its influence on global circulation. Therefore monsoon seasonal prediction has been a goal of forecasters for a long time. Monsoon climate prediction has been attempted in several studies using state-of-the-art dynamic prediction models (Sperber and Palmer 1996; Kang et al. 2002, 2004; Kang and Shukla 2006; Wang et al. 2004, 2005a, b, 2007). However, the dynamical prediction is mainly limited by the nonlinear characteristics of the atmosphere and by the inaccurate performance of current climate models (Kang et al. 2004). The contribution of the internal component to the seasonal mean is larger than that of the external component in monsoon regions where the internal variability arises partly from year-to-year change of intraseasonal variability (ISV) (Sperber et al. 2000; Goswami et al. 2006).

The ISV is one of the most prominent large-scale variability in the tropics (known as Madden–Julian oscillation (MJO), Madden and Julian 1994). In particular, boreal summer ISV plays a crucial role in the evolution of the Asian summer monsoon, including its onset and break through northward propagation over the Indian monsoon region, its northwestward movement over the western Pacific, and its eastward movement along the equator (Yasunari 1979; Lau and Chan 1986; Kang et al. 1989, 1999).

It has been well documented that ISV exhibits a considerable interannual variation (Salby and Hendon 1994; Hendon et al. 1999; Slingo et al. 1999; Sperber et al. 2000; Goswami et al. 2006). The interannual variation of ISV has a practical importance because of its influence on various phenomena like monsoon onset and break in the Asian monsoon regions and because of a close relationship with mean monsoon changes (Yasunari 1979; Lau and Chan 1986; Kang et al. 1989, 1999; Sperber et al. 2000; Goswami and Mohan 2001; Webster and Hoyos 2004; Hoyos and Webster 2006). Observational studies have shown that a strong (weak) monsoon is associated with a higher probability of the occurrence of active (break) conditions (Sperber et al. 2000; Goswami and Mohan 2001; Goswami et al. 2006). Especially, recent studies show that the seasonal mean is highly correlated with the amplitude of ISV activity from observational (Goswami et al. 2006) and modeling studies (Waliser et al. 2004). Moreover, they are closely linked to each other from the viewpoint of predictability as well. Waliser et al. (2003) found that active ISV is related to large intra-ensemble variance (internal variability) which leads to low predictability of the seasonal mean. Therefore, it is noted that the nonlinearity of the ISV is related to the seasonal mean to some degree and the proper simulation of ISV has the potential to improve monsoon predictability.

Because the seasonal mean monsoon is governed by a slowly varying external component of forcing (e.g., ENSO) (Philander 1990; Kang et al. 2004), the interannual variation of ISV may have ENSO-related variability as well. There are a few studies on the interannual variation of ISV and its relationship with SST variations, particularly the ENSO, but the results have remained controversial. Most of the studies demonstrate that overall ISV activity is uncorrelated with SST variations (Salby and Hendon 1994; Hendon et al. 1999; Slingo et al. 1999; Lawrence and Webster 2001). Salby and Hendon (1994) examined the Madden–Julian Oscillation (MJO, Madden and Julian 1994) activity based on wavenumber–frequency filtering and could not find any relationship with ENSO. Hendon et al. (1999) focused on the boreal winter MJO and found the year-to-year variation of MJO intensity to be uncorrelated with ENSO. Slingo et al. (1999) used the variance of the intraseasonally filtered zonal mean wind at 200 mb as a measure of MJO activity and found no significant relationship between the MJO intensity and ENSO.

In contrast to these studies for boreal winter, the linkage between ISV activity and ENSO has been explained in term of an ENSO-induced easterly vertical wind shear mechanism in Teng and Wang (2003) for boreal summer. They found that the strongest interannual variations of ISV are found in the western North Pacific where the westward and northward propagating waves are enhanced based on an increased easterly vertical shear in developing El Nino years. However, there is no model-based study to examine whether the above relationship can be represented in GCMs and exploited in predictions. Therefore, we need to examine if a model can demonstrate interannual ISV predictability that could be traced to interannual SST anomalies, and thus has potential for prediction. Moreover, the predictability can be improved if the model errors are systematic and related to the external SST forcing (Kang et al. 2004). If the interannual variation of ISV is closely linked to external forcing and therefore predictable, it has the potential to influence the seasonal prediction as well.

Based on the aforementioned consideration, the objective of this study is to address the following questions: Is the interannual variation of ISV purely chaotic or is it related to a slowly varying external forcing like ENSO? In the latter case, could the predictability of the interannual variation of ISV be improved by statistical correction methods? To address these questions, we used historical prediction data from ten state-of-the-art climate prediction models.

This study has two significant differences from previous intercomparison studies. One is the use of retrospective forecasts (hindcasts), and the other is the use of coupled models. There are many intercomparison studies that have used AMIP-type simulation only to examine the performance of ISV simulation and cannot relate to real forecasting directly (Slingo et al. 1996; Kang et al. 2002; Waliser et al. 2003). In contrast, this study uses retrospective forecasts from ten state-of-the-art coupled climate prediction models for the 21 years of 1981–2001. Moreover, most of the previous intercomparison studies use atmospheric-only GCMs. However, recent observational and modeling studies suggest that air–sea coupling on intraseasonal timescales is important for the maintenance of ISV and incorporating the coupled processes improves ISV simulation in terms of its intensity, propagation, seasonality and predictability (Wang and Xie 1998; Waliser et al. 1999; Woolnough et al. 2000; Kemball-Cook et al. 2002; Webster et al. 2002; Fu et al. 2003, 2006; Fu and Wang 2004; Zheng et al. 2004; Wang et al. 2005a, b). Based on the need for a reassessment of the ISV characteristics in coupled models, this study uses ten state-of-the-art

climate prediction models that include fully coupled atmosphere–ocean processes.

The aim of this study is to investigate whether the interannual ISV is related to the external forcing component, particularly ENSO, and is thus predictable. It begins with a description of the datasets in Sect. 2. The relationship between interannual variations of ISV and ENSO is examined in Sect. 3. Section 4[k1] describes the method for statistical correction and compares the predictability before and after correction. Section 5 summarizes and discusses the results.

2 Experimental framework and data sources

The analysis is based on historical prediction data of fully coupled atmosphere–ocean-land seasonal prediction systems from the following two international projects: The Asia-Pacific Economic Cooperation Climate Center/Climate Prediction and its Application to Society (APCC/CliPAS) (Wang et al. 2007) and "Development of a European Multi-Model Ensemble System for Seasonal to Inter-Annual Prediction" (DEMETER) (Palmer et al. 2004). DEMETER is known to offer better prediction skills over the globe compared with the uncoupled systems (Kang and Shukla 2006).

A description of the experiments is shown in Table 1. The hindcasts for the period 1981–2001 will be discussed in this paper, because it is the common period for which the participating coupled models have generated hindcasts. All models have hindcast with 6- to 9-month integrations for 3–15 different initial conditions. In order to assess seasonal dependence on skill, the hindcasts were started from the initial conditions on 1 February, 1 May, 1 August, and 1 November except for the CFS model, in which the 15 atmospheric initial conditions were taken on the 9, 10, 11, 12, 13, 19, 20, 21, 22, and 23 of the month prior to the target month, and on the last 2 days of the previous month, as well as the first-to-third days of the target month (Saha et al. 2006). We focus on the boreal summer that is defined as May through August with 25 pentads per year.

In order to extract the ISV component, a 20–90 days band-pass filter is applied to each pentad anomaly that has been computed from the 1981 to 2001 pentad climatology for reanalysis and each simulation, respectively. The filter is a symmetric, four-pole, low-pass, tangent Butterworth filter (Oppenheim and Schafer 1975). The filter is applied, first retaining timescales longer than 20 days and then retaining timescales longer than 90 days. The bandpass data are obtained by subtracting the two filtered datasets. The end-point effect is reduced by extending the ends of the series by duplicating the beginning and ending values.

Table 1 Description of atmosphere and ocean models

Acronym names	Institute	AGCM	Resolution	OGCM	Resolution	Period	Integration (months)	Ensembles	References
CERF	CERFACS	ARPEGE	T63 L31	OPA 8.2	2.0 × 2.0 L30	1980–2001	6	9	Palmer et al. (2004)
ECMW	ECMWF	IFS	T95 L40	HOPE-E	1.4 × 0.3–1.4 L29	1958–2001	6	9	
INGV	INGV	ECHAM-4	T42 L19	OPA 8.1	2.0 × 0.5–1.5 L31	1973–2001	6	9	
LODY	LODYC	IFS	T95 L40	OPA 8.2	2.0 × 2.0 L31	1974–2001	6	9	
METF	Meteo France	ARPEGE	T63 L31	OPA 8.0	182 × 152 GP L31	1958–2001	6	9	
MAXP	MPI	ECHAM-5	T42 L19	MPI-OM1	2.5 × 0.5–2.5 L23	1969–2001	6	9	
UKMO	UK Met Office	HadAM3	2.5 × 3.75 L19	GloSea OGCM	1.25 × 0.3–1.25 L40	1959–2001	6	9	
SNU	SNU	SNU	T42 L21	MOM2.2	1/3° × 1° L32	1960–2004	7	5	Kug et al. (2007)
NCEP	NCEP	GFS	T62 L64	MOM3	1/3° × 1° L40	1981–2003	8	15	Saha et al. (2006)
NASA	NASA	NSIPP1	2° × 2.5° L34	Poseidon V4	1/3° × 5/8° L27	1980–2004	6	3	Vintzileos et al. (2003)

All data were interpolated to a spatial resolution of 2.5° latitude × 2.5° longitude. The observational datasets for verification are obtained from the Climate Prediction Center Merged Analysis of Precipitation (CMAP) (Xie and Arkin 1997). Zonal winds at 850 and 200 hPa are from the National Center for Environmental Prediction/National Center for Atmospheric Research (NCEP/NCAR) reanalysis (Kalnay et al. 1996) and SST data were obtained from NCEP (Reynolds and Smith 1994).

3 Interannual variations of ISV and its relationship with ENSO

To examine the interannual variation of ISV, the ISV activity (σ_y) is defined as:

$$\sigma_y^2 = \frac{1}{P(E-1)} \sum_{p=1}^{P} \sum_{e=1}^{E} (x_{ype} - \overline{x_e})^2,$$

where x_{ype} is precipitation anomaly, y year, p pentad number relative to the initial forecast date (P = 25), and e ensemble member. Overbar denotes the climatological (21 years) mean of filtered precipitation anomalies. Therefore, ISV activity indicates the ensemble mean intensity of ISV, which varies from year to year. To reduce the errors associated with the uncertainties in model physical parameterization and to make an effective way to aggregate and synthesize the model outputs, the model composite $\left(\overline{\sigma_y}\right)$ is calculated as:

$$\overline{\sigma_y^2} = \frac{1}{M} \sum_{m=1}^{M} (\sigma_{ym}^2),$$

where m number of the model (M = 10).

Figure 1 shows the distribution of climatological ISV activity which is obtained by 21-year averaged ISV activity (σ_y), from observation and the model composite, respectively. The largest amplitude of the observed ISV activity exists around the Philippine Sea, the Bay of Bengal, and over the eastern Arabian Sea. The model composite shows a pattern broadly similar to observation. However, it underestimates the variability in the equatorial eastern Indian Ocean and the western Pacific considerably, which has been one of the main problems for GCMs (Slingo et al. 1996; Kang et al. 2002; Waliser et al. 2003).

The interannual variation of ISV activity is examined by the standard deviation of the ISV activity anomalies during each summer for 21 years. Although the climatological ISV activity is strong in the Bay of Bengal, its interannual variation is weaker than in the western North Pacific (WNP) (Fig. 2a). The WNP shows the most pronounced

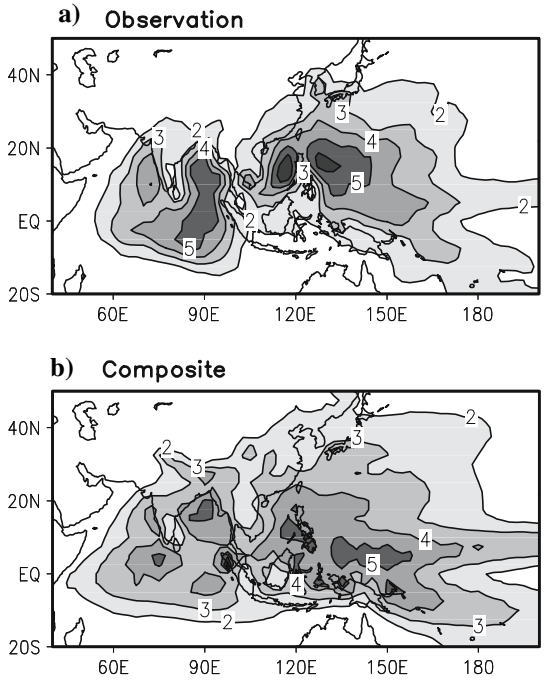

Fig. 1 Distributions of the climatological ISV activity for the **a** observation and **b** model composite. The unit is mm day^{-1}

interannual variations. Teng and Wang (2003) showed similar results and have demonstrated that the strongest interannual variations in ISV activity found in the WNP result from enhanced westward and northward propagating waves in the ENSO developing summer. Figure 2b is the corresponding pattern of the model composite. In the model composite, the interannual variation is limited in the central equatorial Pacific and has no significant value over the Indian monsoon region or over the WNP where the dominant interannual change is exhibited in the observational field. The performance of each model in simulating the interannual variation of ISV activity is examined and shows a variety of spatial patterns (Fig. 2c–l). Although there are some differences between the models, most of them simulate excessive variation in the central tropical Pacific and fail to reproduce the largest variability in the WNP region. We note that there are difficulties in simulating the interannual changes of ISV using recent climate prediction models even though the atmosphere–ocean coupled process is included in them.

To know the systematic bias in model simulations and to understand the main factor that controls interannual variations in ISV, EOF analysis was applied to the observed and simulated ISV activity anomaly. Compared to the large standard deviation of ISV activity that is located over the WNP in observation (Fig. 2a), the first EOF mode of ISV activity that explains 14.47% of the total variance is characterized by large positive components over the central

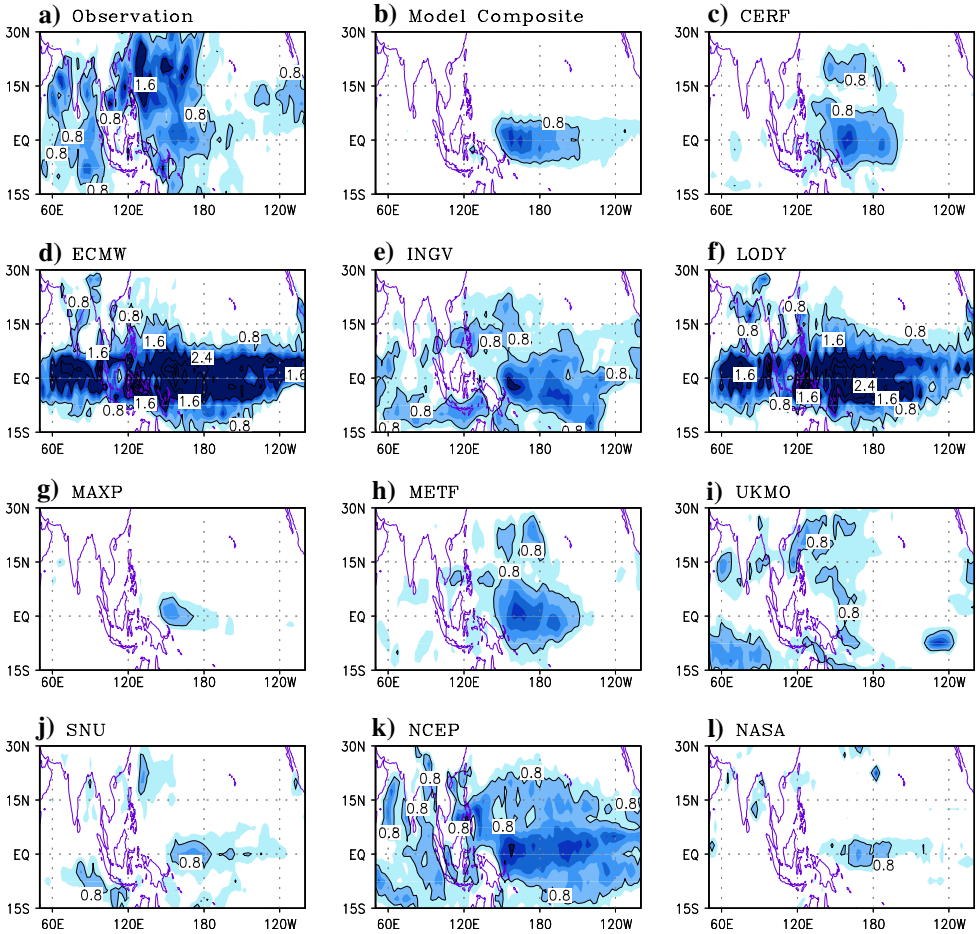

Fig. 2 Interannual standard deviations of the boreal summer ISV activity in **a** observation, **b** model composite, and **c–l** various models. Contour interval is 0.8 mm day^{-1} and *shadings* indicate the standard deviation more than 0.6 mm day^{-1}

western Pacific with maxima between 10°S and 10°N (Fig. 3a). The first mode of the model composite (Fig. 3c), that accounts for 47.61% of the total variance, produces the large variability over the central western Pacific that corresponds with its standard deviation reasonably well (Fig. 2b). Figure 4 exhibits the eigenvector of the first EOF for individual models, indicating a large variability of systematic error in simulated spatial patterns among models. The second eigenvectors of the observation and model composite explain 11.18 and 24.40% of total variance, respectively (Fig. 3b, d). In observation (Fig. 3b), the spatial pattern is characterized by large variations in the WNP, which is similar to the standard deviation of ISV activity (Fig. 2a).

For the first and second mode, the spatial patterns of the model counterpart show a great difference from observation. However, the time series of principal components (PC) associated with the eigenvectors, shown in Fig. 3e and f, vary in a similar way to observation. In particular, the PC time series of the first mode is well correlated to the Nino3.4 index. Therefore, it is noted that the first mode is related to ENSO SST anomalies. The similarity between the observed and predicted PC time series provides possibilities for model error correction using a statistical approach.

To examine how well individual models simulate the ENSO-related variability, the pattern correlation of the first EOF eigenvector (Fig. 4) over the ENSO-monsoon region (40°–300°E and 20°S–30°N) and the temporal correlation of the first PC time series between observation and the model were computed (Fig. 5). The most of model have some difficulties in capturing the spatial distribution of the observed first mode showing the pattern correlation coefficients ranging from 0.32 (for INGV model) to 0.67 (Met France model) (Fig. 5, black shading). Although EOF spatial patterns in the models are somewhat different from observation (Fig. 4), a similarity exists between the PC time series of observed and predicted modes (Fig. 5, diagonal shading). Therefore, prediction models have the ability to capture the prominent mode of ISV activity corresponding to ENSO even if the spatial pattern is slightly different from observation.

To investigate the relationship between ISV activity and forced SST variation, the correlation coefficient between the first EOF time series and the Nino 3.4 index from its own model output was computed (Fig. 5, gray shading). In

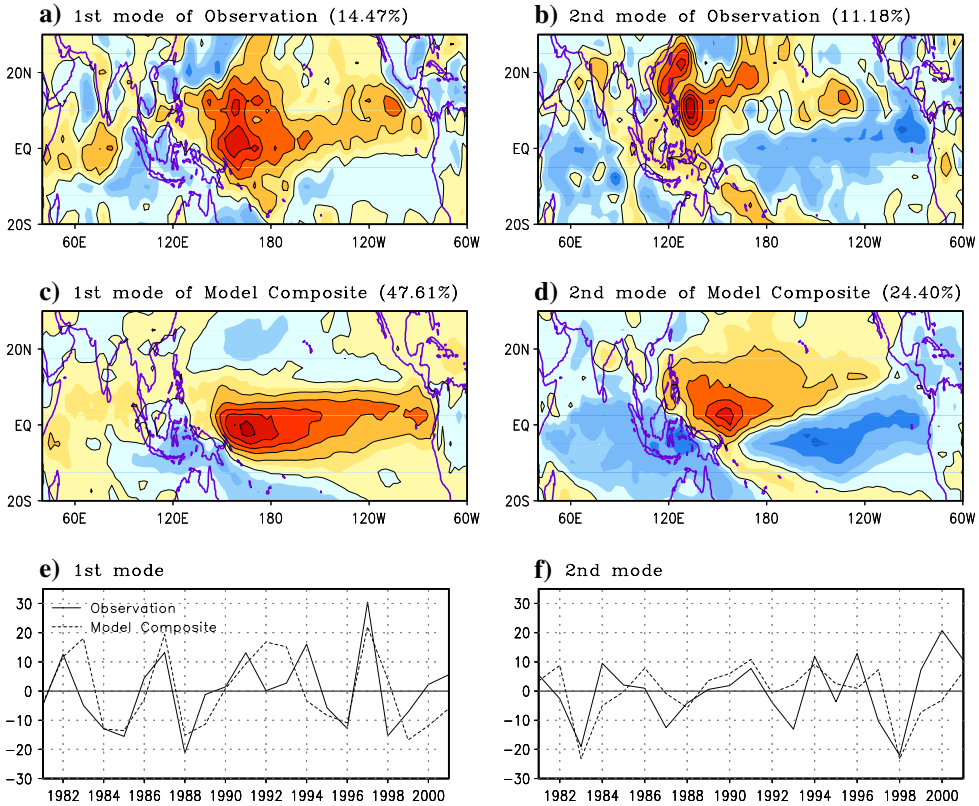

Fig. 3 The first and second EOF modes of the observed and model composite ISV activity. **a**, **b** The observed first and second eigenvectors; **c**, **d** the simulated counterparts. *Shading* indicates positive value and contour interval is 0.02. **e**, **f** The time series associated with the eigenvectors. *Solid* and *dashed lines* indicate the observed and simulated time series, respectively

general, most models simulate well the relationship between the first mode of ISV activity and the model Nino 3.4 SST. Even the models that have difficulty in representing the leading vectors exhibit a close relationship between ISV activity and their own SST variability. In the second mode that is supposed to have a much more significant effect on the monsoon region in observation, the spatial patterns of the predicted eigenvectors are different from observation but the interannual variation of the predicted PC timeseries are similar to the observed counterpart like the first mode (not shown).

The linkage between ISV activity and ENSO can be explained by the ENSO-induced easterly vertical wind shear mechanism (Teng and Wang 2003). Previous studies have shown that the easterly vertical shear can enhance Rossby waves in the lower troposphere and the enhanced low-level perturbation increases moisture convergence at the boundary layer and amplifies the moist equatorial Rossby waves (Wang and Xie 1996; Xie and Wang 1996). The enhanced shear in the western Pacific enhances the development and northwestward emanation of Rossby waves in the lower troposphere effectively, and then the ISV is reinforced in the western Pacific. On the other hand, in the Indian Ocean, the ENSO-induced wind shear is too weak to affect the mean circulation. Therefore, ISV activity is insensitive to ENSO in the Indian monsoon region.

To examine the robust relationship between the ISV activity and ENSO-induced wind shear in individual models, we applied the regression analysis. Before the regression analysis, we made the summer mean easterly vertical wind shear (u_{850}–u_{200}) for each individual year in observation and model composite, respectively. Then, we obtained the regression coefficient for ISV activity and mean vertical wind shear by a linear regression method with respect to the observed and simulated Nino 3.4 SST, respectively. Figure 6a and b show the regression coefficients of ISV activity and Fig. 6c and d the wind shear.

The western Pacific, which is a climatologically transition region of wind shear has a pronounced interannual variation associated with ENSO—a strong easterly vertical shear—both in observation and in the model composite (Fig. 6c, d). Because of the weak vertical shear in the mean state (not shown) over the western Pacific, it is easier to reverse the sign of the vertical wind shear in the ENSO season. It is noted that the enhanced vertical shear region is similar to the ENSO-induced ISV active region (Fig. 6a, b). The enhanced waves promote the northward and northwestward propagating waves and reinforce the ISV in the WNP.

Although this study offers explanations on ENSO-induced ISV activity over the WNP region, a number of issues remain to be addressed. In some models (ECMWF, LODYC, UKMO, and NCEP), there is a strong interannual

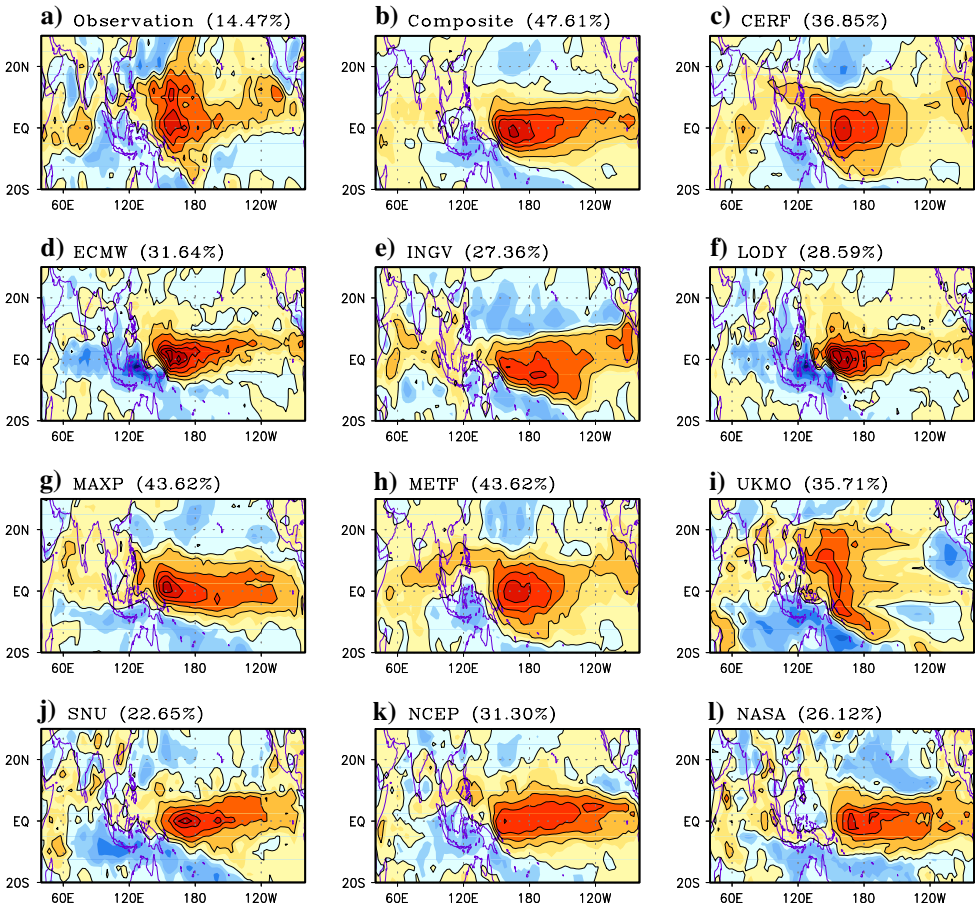

Fig. 4 The first EOF mode of the ISV activity in **a** observation, **b** model composite, and **c–l** various models. *Shading* indicates positive value and contour interval is 0.02

modulation of ISV activity over the Indian Ocean (Fig. 2). Moreover, the spatial pattern of the first EOF eigenvector (Fig. 4) and strong correlation between first PCs and Nino 3.4 time series (Fig. 5) would mean a strong interannual modulation of ISV by ENSO over the eastern Indian Ocean. Note that over the eastern Indian Ocean, the anomalous anti-Walker circulation during El Nino events tends to suppress the convection over the eastern equatorial Indian Ocean, thus the ISV there should be significantly affected. The ISV in the off-equatorial Indian monsoon region is different. In the off-equatorial Indian monsoon region, the change of vertical shear is relatively small during ENSO—less than 10% of the climatological value. Thus, the changes in vertical shear cannot significantly

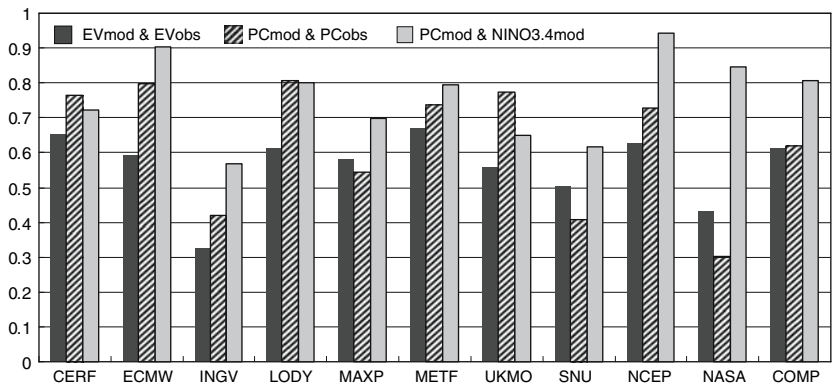

Fig. 5 Pattern correlation coefficients of the first EOF eigenvectors between the observed and associated model ISV activity over the ENSO-monsoon region (40°–300°E and 20°S–30°N; *black shaded bar*), correlation coefficients of the first EOF time series between observation individual model (*diagonal shaded bar*), and correlation coefficients between the first EOF time series of each model and its own Nino 3.4 index (*gray shaded bar*)

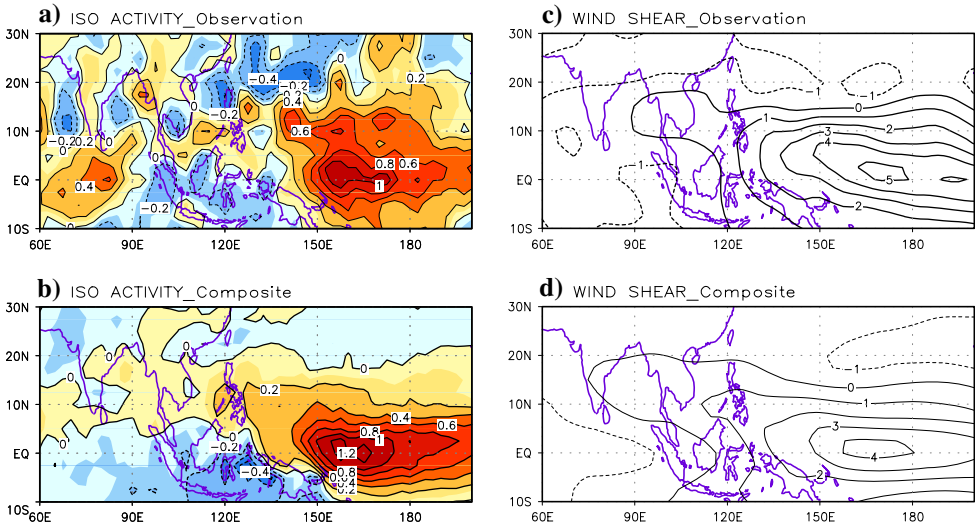

Fig. 6 Regression coefficients of ISV activity (*left*) for the **a** observation and **b** model composite, and coefficients of summer mean u_{850}–u_{200} vertical wind shear (*right*) for the **c** observation and **d** model composite

affect the interannual variability of ISV there. Moreover, even though these models reproduce more realistic amplitude of interannual variability in ISV, they have a model-dependent systematic bias in their spatial pattern of variability (Fig. 4). Especially, ECMWF and LODYC show opposite sign of ISV variation compared to observation over equatorial western Indian Ocean. Although some models show significant amplitude as observed value in Indian Ocean, the spatial pattern has systematic bias, and therefore statistical correction plays important role.

4 Predictability of ISV activity after systematic bias correction

Models still have problems in simulating the ISV activity in monsoon regions even when they include the atmosphere–ocean coupled process. Although the models have difficulty in simulating the spatial variability of ISV activity, they have the ability to capture the temporal variability, which is related to the SST boundary forcing. Therefore, the predictability can be improved by statistical correction since the model errors are systematic and related to external forcing. In previous studies these errors were shown to be correctable by a close statistical relationship between observation and model prediction (Kang et al. 2004). In spite of the poor simulation of the EOF spatial pattern, the similarity between the time series of observed and predicted modes offers the possibility of error correction (Fig. 3e, f). The difference in spatial patterns can be corrected by replacing the model eigenmodes with the corresponding observed modes.

A statistical correction method is applied to reduce the systematic error for individual models based on the SVD method (Feddersen et al. 1999; Kang et al. 2004). The correction is performed by replacing the coupled pattern of forecasts with that of observations which are temporarily correlated. Because the normalized principal component of forecasts and observations is used in construction of the covariance matrix to be solved by SVD, it is the same as the Canonical Correlation Analysis (CCA) (Bretherton et al. 1992). The spatial pattern of leading CCA modes is used, and the transfer function for the replacement is as follows:

$$F(x,t) = \sum_{i=1}^{m} \alpha_i Y_i(t) R_i(x),$$

where $F(x,t)$ is corrected field, $Y_i(t)$ time coefficient of the CCA mode of forecast and $R_i(x)$ CCA pattern of observation. i is the number of the mode and ten leading modes are used (m = 10) because the sum of the first ten modes explains more than 90% of the total variance. α_i is weighting coefficient based on the correlation coefficient between the CCA time series of observation and forecast. Therefore, the leading modes have more weight. Once the CCA patterns and weighting coefficients are determined by the training dataset, the time coefficient $Y_i(t)$ of the target forecast is obtained by projecting the CCA pattern of the forecast onto the model forecast filed. A detailed description of statistical correction can be found in Kang et al. (2004). A cross-validation method is applied to each year.

The prediction skill of ISV activity can be measured by the anomaly correlation between predictions and the corresponding observations for 21 years. The predictability of the model composite is computed by averaging the predicted field after correction for ten models. Figure 7 shows the prediction skill of the model composite before and after error correction. ISV activity is predictable only in the Tropics before correction but is improved across the whole

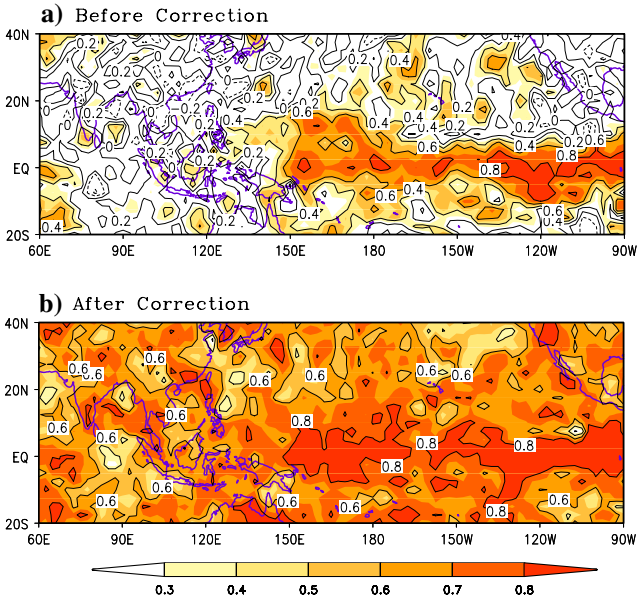

Fig. 7 Distribution of the correlation coefficient between the observed and the predicted ISV activity of the model composite for **a** before and **b** after correction. Contour interval is 0.2

globe after correction. The predictability is also examined through the 21-year-averaged spatial pattern correlation averaged over the Asian monsoon regions (60°–180°E and 10°S–30°N) for each model (Fig. 8). All models exhibit enhanced predictabilities and the model composite changes from 0.25 to 0.65 after correction. To examine more clearly the enhancement of predictability after correction, the ISV activity index is defined by the area-averaged ISV activity anomaly over the WNP (100°–150°E and 10°–30°N) where the interannual variation of ISV activity is dominant. Figure 9 shows the time correlation coefficient of the ISV activity index, before and after error correction. The predictability of ISV activity index is enhanced except in INGV. Negative correlations change to positive in some models (e.g., CERF, MAXP, UKMO, and NCEP), and low correlations have relatively large positive values after correction (e.g., ECMW, SNU, and NASA). The predictability of the model composite ISV activity index changes from 0.03 to 0.48 after correction.

In this study, a cross-validation method is applied to each year. However, when a statistical forecast or correction methodology is to be applied to real time forecasts or correction of anomalies, adequate cross-validation becomes essential as no information of future values exists for performing the real time training. The de-correlation time scale defines a sufficiently large window for the cross-validation process. For interannual variability this window is of the order of 2–3 years. Therefore, we re-compute Fig. 8 by cross-validation with removal of 1 year prior, the year in consideration, and one year after. By comparison between Fig. 8 and re-computed results (not shown), we notice that improvements accomplished by the proposed statistical correction technique are very dependent on the cross-validation window. For example, for the model composite, the corrected correlation drops from 0.65 to 0.44 when the 3-year cross-validation window is used. Therefore, the sensitivity of the cross-validation window should be considered for applying the statistical correction method.

5 Summary and discussion

Reproducibility of the boreal summer (MJJA) intraseasonal variability (ISV) and its interannual variation related to ENSO in coupled climate prediction models are evaluated by diagnosing 21-year hindcast outputs from ten state-of-the-art prediction models that participated in the APCC/CliPAS and DEMETER projects.

There are two sensitivity tests with the dataset. One is about the choice of cut-off frequency. To extract the ISV component, a 20–90 days filter is applied to pentad precipitation anomalies. Through an examination of the sensitivity of the cut-off frequency with daily data that is available in hindcasts, it is concluded that the interannual variability of ISV related to ENSO is not sensitive to the choice of cut-off frequency if the frequency range is within

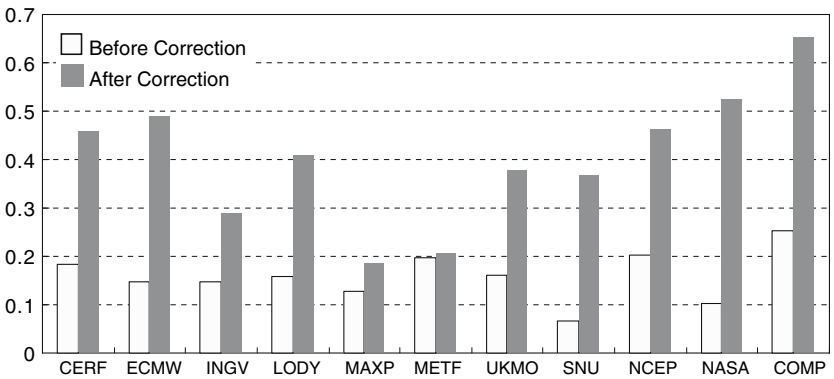

Fig. 8 21-year-averaged pattern correlation coefficients between the observed and predicted ISV activity before (*open bar*) and after (*shaded bar*) the correction over the Asian monsoon regions (60°–180°E and 10°S–30°N)

10–100 days. The other is the sensitivity of the period defined as "summer". With increasing lead time, the mean state of each model drifts towards its own climatology and we stated the interannual variation of ISV is linked with the mean state. As a result, the characteristics of the ISV may be lead time dependant. However, the difference in the variance characteristics (Figs. 1, 2, 3) is not distinctive over the MJJ or JJA periods instead of the MJJA period.

The observed climatological ISV activity for the MJJA period exhibits its largest values over the western North Pacific and Indian monsoon regions. The interannual variation of ISV activity is primarily found over the western North Pacific in observation, while most models have the largest variability over the central tropical Pacific and exhibit a large range of spatial patterns that are different from observation. However, the leading EOF modes of ISV activity in the models are closely linked to the model's El Nino-Southern Oscillation (ENSO). This feature resembles the observed ISV and ENSO relationship. The ENSO-induced easterly vertical shear anomalies in the western and central tropical Pacific, where the summer mean vertical wind shear is weak, result in ENSO-related changes in ISV activity in both the observation and the models. In the Indian monsoon region, ENSO-induced wind shear is too weak to affect the mean circulation and thus the ISV activity is insensitive to ENSO.

A close relationship in the temporal variations of the dominant modes of ISV activity exists between the observation and models. Thus, a statistical correction method based on singular value decomposition is designed. It is shown that this method is able to remove a large portion of the systematic errors. After the bias correction, the predictability is enhanced, especially in the western Pacific. The 21-year-averaged pattern correlation skill changes from 0.25 to 0.65 over the entire Asian monsoon region after applying the bias correction to the multi-model ensemble mean prediction.

The improved predictability of the ISV activity offers a possibility of an improvement in seasonal prediction because of the close relationship between the ISV and seasonal mean state, as mentioned in the introduction. Figure 10 exhibits the relationship between the mean state and ISV activity in terms of predictability. The predictability can be measured by the spatial correlation between the predicted ISV activity anomaly and the corresponding observation over the Asian monsoon region (40°–180°E and 20°S–30°N) and then averaged for 21 years (the vertical axis in Fig. 10). The predictability is generally low compared to the predictability of the summer mean obtained in the same way (the horizontal axis in Fig. 10). The figure shows a very close relationship between the predictability of the mean field and the ISV activity which is correlated at a level of 0.92. Most of the state-of-the-art climate prediction models still have difficulty in simulating even the seasonal mean state and its interannual variations (Sperber and Palmer 1996; Kang et al. 2002; Kang and Shukla 2006). The results of this study suggest that this can be partly overcome by the improvement in the predictability of ISV activity. The way to link these two variables remains as a subject for further study.

It has been emphasized that the air–sea interactions are important for ISV simulation, and especially for ISV prediction (Fu et al. 2006). In order to fully understand the importance of air–sea coupling in ISV prediction, not only on an interannual timescale but also on a daily timescale, a

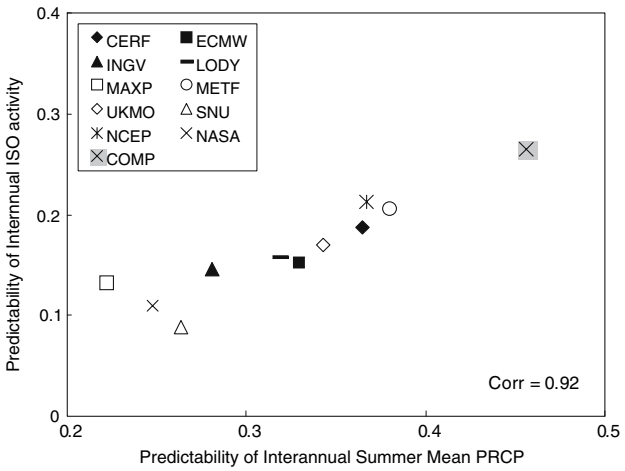

Fig. 10 Scatter plot of predictability on summer mean precipitation (*horizontal axis*) and ISV activity (*vertical axis*) over the Asian monsoon region (40°–180°E and 20°S–30°N). The correlation is 0.92

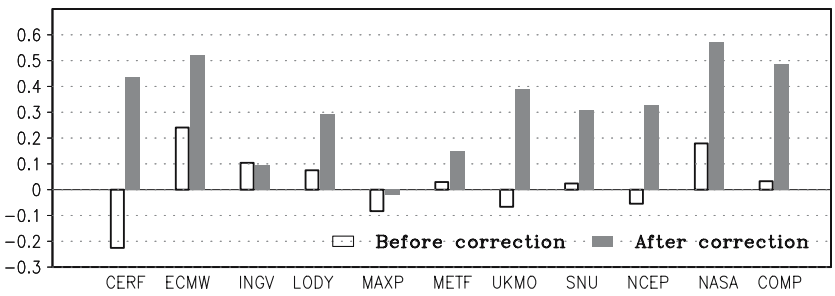

Fig. 9 Correlation coefficients between the observed and predicted ISV activity index before (*open bar*) and after (*shaded bar*) the bias correction

comparison study with coupled and uncoupled models will be carried out in further work.

Acknowledgments This research has been supported by the SRC program of Korea Science and Engineering Foundation, and the Ministry of Environment as "The Ecotechonopia 21 Project", and the second stage of the Brain Korea 21 Project. The third and fourth authors were supported by APEC Climate Center (APCC) as a part of APCC International research project.

References

Bretherton CS, Smith C, Wallace JM (1992) An intercomparison of methods for finding coupled pattern in climate data. J Clim 5:541–560

Feddersen H, Navarra A, Ward MN (1999) Reduction of model systematic error by statistical correction for dynamical seasonal prediction. J Clim 12:1974–1989

Fu X, Wang B, Li T, McCreary JP (2003) Coupling between northward propagation, intraseasonal oscillations and sea surface temperature in the Indian Ocean. J Atmos Sci 60:1733–1753

Fu X, Wang B (2004) Differences of boreal summer intraseasonal oscillations simulated in an atmosphere–ocean coupled model and an atmosphere-only model. J Clim 17:1263–1271

Fu X, Wang B, Waliser DE, Tao L (2006) Impact of atmosphere–ocean coupling on the predictability of monsoon intraseasonal oscillations. J Atmos Sci 64:157–174

Goswami BN, Mohan RSA (2001) Intraseasonal oscillations and interannual variability of the Indian summer monsoon. J Clim 14:1180–1198

Goswami BN, Wu G, Yasunari T (2006) The annual cycle, intraseasonal oscillations, and roadblock to seasonal predictability of the Asian summer monsoon. J Clim 19:5078–5099

Hendon HH, Zhang C, Glick J (1999) Interannual fluctuations of the Madden–Julian oscillation during austral summer. J Clim 12:2538–2550

Hoyos CD, Webster PJ (2007) The role of intraseasonal variability in the nature of Asian Monsoon Precipitation. J Clim (in press)

Kalnay E, Kanamitsu M, Kistler R, Collins W, Deaven D, Gandin L, Iredell M, Saha S, White G, Woollen J, Zhu Y, Chelliah M, Ebisuzaki W, Higgins W, Janowiak J, Mo KC, Ropelewski C, Wang J, Leetmaa A, Reynolds R, Jenne R, Joseph D (1996) The NCEP/NCAR 40-year reanalysis project. Bull Am Meteorol Soc 77:437–471

Kang I-S, An SI, Joung CH, Yoon SC, Lee SM (1989) 30–60 day oscillation appearing in climatological variation of outgoing longwave radiation around East Asia during summer. J Korean Meteorol Soc 25:149–160

Kang I-S, Ho CH, Lim YK (1999) Principal modes of climatological seasonal and intraseasonal variations of the Asian summer monsoon. Mon Weather Rev 127:322–340

Kang I-S, Jin K, Wang B, Lau KM, Shukla J, Schubert SD, Waliser DE, Krishnamurthy V, Stern WF, Satyan V, Kitoh A, Meehl GA, Kanamitsu M, Galin VY, Kim JK, Sumi A, Wu G, Liu Y (2002) Intercomparison of the climatological variations of Asian summer monsoon precipitation simulated by 10 GCMs. Clim Dyn 19:383–395

Kang I-S, Lee J-Y, Park C-K (2004) Potential predictability of summer mean precipitation in a dynamical seasonal prediction system with systematic error correction. J Clim 17:834–844

Kang I-S, Shukla J (2006) Dynamic seasonal prediction and predictability of the monsoon. In: Wang B (ed) The Asian monsoon. Springer-Praxis, Chichester

Kug J-S, Kang I-S, Choi D-H (2007) Seasonal climate predictability with tier-one and tier-two prediction systems. Clim Dyn. doi:10.1007/s00382-007-0264-7

Kemball-Cook SR, Wang B, Fu X (2002) Simulation of the intraseasonal oscillation in the ECHAM4 model: the impact of coupling with an ocean model. J Atmos Sci 59:1433–1453

Lau KM, Chan PH (1986) Aspects of the 40–50 day oscillation during the Northern summer as inferred from outgoing longwave radiation. Mon Weather Rev 114:1354–1367

Lawrence DM, Webster PJ (2001) Interannual variations of the intraseasonal oscillation in the South Asian summer monsoon region. J Clim 14:2910–2922

Madden RA, Julian PR (1994) Detection of a 40–50 day oscillation in the zonal wind in the tropical Pacific. Mon Weather Rev 122:813–837

Oppenheim, AV, Schafer RW (1975) Digital signal processing, p 585. Prentice Hall, Englewood Cliffs

Palmer TN, Alessandri A, Andersen U, Cantelaube P, Davey M, Délé cluse P, Dé qué M, Dı́ ez E, Doblas-Reyes FJ, Feddersen H, Graham R, Gualdi S, Gué ré my J-F, Hagedorn R, Hoshen M, Keenlyside N, Latif M, Lazar A, Maisonnave E, Marletto V, Morse AP, Orfila B, Rogel P, Terres J-M, Thomson MC (2004) Development of a European multimodel ensemble system for seasonal-to-interannual prediction (DEMETER). Bull Am Meteor Soc 85:853–872

Philander SGH (1990) El Nino, La Nina, and the southern oscillation, p 293. Academic Press, London

Reynolds RW, Smith TM (1994) Improved global sea surface temperature analysis using optimum interpolation. J Clim 8:929–948

Saha S et al (2006) The NCEP climate forecast system. J Clim 19:3483–3517

Salby ML, Hendon HH (1994) Intraseasonal behavior of clouds, temperature, and motion in the Tropics. J Atmos Sci 51:2207–2224

Slingo JM, Sperber KR, Boyle JS, Ceron JP, Dix M, Dugas B, Ebisuzaki W, Fyfe J, Gregory D, Gueremy JF, Hack J, Harzallah A, Inness P, Kitoh A, Lau WKM, McAvaney B, Madden R, Matthews A, Palmer TN, Park CK, Randall D, Renno N (1996) Intraseasonal oscillations in 15 atmospheric general circulation models: results from an AMIP diagnostic subproject. Clim Dyn 12:325–357

Slingo JM, Rowell DP, Sperber KR, Nortley F (1999) On the predictability of the interannual behavior of the Madden–Julian oscillation and its relationship with El Nino. Q J R Meteorol Soc 125:583–609

Sperber KR, Palmer TN (1996) Interannual tropical rainfall variability in general circulation model simulations associated with atmospheric model intercomparison project. J Clim 9:2727–2750

Sperber KR, Slingo JM, Annamalai H (2000) Predictability and the relationship between subseasonal and interannual variability during the Asian summer monsoon. Q J R Meteorol Soc 126:2545–2574

Sperber KR (2004) Madden–Julian variability in NCAR CAM2.0 and CCSM2.0. Clim Dyn 23:259–278

Sperber KR, Gualdi S, Legutke S, Gayler V (2005) The Madden–Julian oscillation in ECHAM4 coupled and uncoupled general circulation models. Clim Dyn 25:117–140

Teng H, Wang B (2003) Interannual variations of the boreal summer intraseasonal oscillation in the Asian-Pacific region. J Clim 16:3572–3584

Vintzileos A, Rienecker MM, Suarez M, Miller S, Pegion P, Bacmeister J (2003) Simulation of the El Nino-southern oscillation phenomenon with NASA's seasonal-to-interannual prediction project coupled general circulation model. CLIVAR Exch 8:25–27

Wang B, Xie XS (1996) Low-frequency equatorial waves in vertically sheared zonal flow. Part I: stable waves. J Atmos Sci 53:449–467

Wang B, Xie XS (1998) Coupled modes of the warm pool climate system. Part 1: the role of air–sea interaction in maintaining Madden–Julian oscillation. J Clim 11:2116–2135

Wang B, Kang I-S, Lee J-Y (2004) Ensemble simulations of Asian–Australian monsoon variability by 11 AGCMs. J Clim 17:803–818

Wang B, Ding Q, Fu XH, Kang I-S, Jin K, Shukla J, Doblas-Reyes F (2005a) Fundamental challenge in simulation and prediction of summer monsoon rainfall. Geophys Res Lett 32:L15711

Wang B, Webster PJ, Teng H (2005b) Antecedents and self-induction of active-break south Asian monsoon unraveled by satellites. Geophys Res Lett 32:L04704 (doi:10.1029/2004GL020996)

Wang B, Lee JY, Kang I-S, Shukla J et al (2007) Assessment of the APCC/CliPAS multi-model seasonal hindcast. Clim Dyn (submitted)

Waliser DE, Lau KM, Kim JH (1999) The influence of coupled sea surface temperatures on the Madden–Julian oscillation: a model perturbation experiment. J Atmos Sci 56:333–358

Waliser DE, Jin K, Kang I-S, Stern WF, Schubert SD, Wu MLC, Lau KM, Lee MI, Krishnamurthy V, Kitoh A, Meehl GA, Galin VY, Satyan V, Mandke SK, Wu G, Liu Y, Park C-K (2003) AGCM simulations of intraseasonal variability associated with the Asian summer monsoon. Clim Dyn 21:423–446

Waliser DE, Murtugudde R, Lucas L (2004) Indo-Pacific Ocean response to atmospheric intraseasonal variability. Part II: boreal summer and the intraseasonal oscillation. J Geophys Res 109:C03030 (doi:10.1029/2003JC002002)

Webster PJ, Coauthors (2002) The JASMINE pilot study. Bull Am Meteorol Soc 83:1603–1629

Webster PJ, Hoyos C (2004) Prediction of monsoon rainfall and river discharge on 15–30-day time scales. Bull Am Meteorol Soc 85:1745–1765

Woolnough SJ, Slingo JM, Hoskins BJ (2000) The relationship between convection and sea surface temperature on intraseasonal timescales. J Clim 13:2086–2104

Xie X, Wang B (1996) Low-frequency equatorial waves in vertically sheared zonal flow, Part II: unstable waves. J Atmos Sci 53:3589–3605

Xie P, Arkin PA (1997) Global precipitation: a 17-year monthly analysis based on gauge observations, satellite estimates, and numerical model outputs. Bull Am Meteorol Soc 78:2539–2558

Yasunari T (1979) Cloudiness fluctuations associated with the Northern Hemisphere summer monsoon. J Met Soc Jpn 57:227–242

Zheng Y, Waliser DE, Stern W, Jones C (2004) The role of coupled sea surface temperatures in the simulation of the tropical intraseasonal oscillation. J Clim 17:4109–4134